RSC Advances

ROYAL SOCIETY OF CHEMISTRY

www.rsc.org/advances

Journal Name

RSCPublishing

ARTICLE

Self-assembled Asymmetric Membrane Containing Micron-size Germanium for High Capacity Lithium Ion Batteries

Cite this: DOI: 10.1039/x0xx00000x

Received 00th January 2012,
Accepted 00th January 2012

DOI: 10.1039/x0xx00000x

www.rsc.org/

Ian Byrd,[a] Hao Chen,[b] Theron Webber,[a] Jianlin Li[c*] and Ji Wu,[a*]

Here we report the formation of novel asymmetric membrane electrode containing micron-size (~5 μm) germanium powders through a self-assembly phase inversion method for high capacity lithium ion battery anode. 850 mAh g^{-1} capacity (70%) can be retained at a current density of 600 mA g^{-1} after 100 cycles with excellent rate performance. Such a high retention rate has rarely been seen for pristine micron-size germanium anodes. Scanning electron microscope study reveals that germanium powders are uniformly embedded in a networking porous structure consisting of both nanopores and macropores. It is believed that such a unique porous structure can efficiently accommodate the ~260% volume change during germanium alloying and de-alloying process, resulting in an enhanced cycling performance. These porous membrane electrodes can be manufactured in large scale using a roll-to-roll processing method.

Introduction

High capacity lithium ion batteries (LIBs) have broad applications from static energy storage of intermittent power sources, mobile electronics to electric vehicles.[1-3] Commercial graphite anode for rechargeable LIBs has a limited theoretical capacity of 372 mAh g^{-1}.[3] To further increase the overall capacity of LIBs, alloying anode materials such as silicon and germanium have been extensively explored, mainly due to their attractive high theoretical capacities.[4-8] Compared to silicon, Ge has several advantages as a LIB anode: 1) several orders of magnitude higher in electrical conductivity and lithium ion diffusivity enabling excellent rate performance;[9] 2) particles more robust and thus lower tendency to fracture with similar particle size during the repeating lithiation/de-lithiation process, which has been revealed by recent *in situ* transmission electron microscopy (TEM) studies;[10-12] 3) similar volumetric capacities (7366 Ah L^{-1} for Ge vs. 8334 Ah L^{-1} for Si).[9]

However, Ge, similar to Si, experiences immense volume change (~260%) during lithium intercalation and de-intercalation, which induces huge stress leading to fracture, pulverize, and lose contact with conductive additives. Additionally the unstable solid electrolyte interphase (SEI) consumes lithium metal continuously, leading to a dramatic capacity fade. Quite a few creative strategies have been proposed to overcome the aforementioned volume expansion problem, mainly through various kinds of nanostructuring (nanowires, nanotubes, nanoparticles, microporous and mesoporous materials).[9, 13-17] However, expensive chemical vapour deposition (CVD) technology, risky acid etching, complicated metal reduction and costly catalysts are usually needed to obtain these nanostructures, thus hindering their practical application in large scale. Further, nanomaterials are orders of magnitude more expensive than their micron-size counterparts. Therefore, it is highly desired to use micron-size Ge and Si powders in LIBs. Unfortunately, the cycling performance of micron-size Si and Ge is extremely poor, and very few successful cases have been reported so far.[18-20] Cui et al. utilized various glues to enhance the cycling performance of micron-size silicon using either extremely thin coating (~3 μm thick)[20] or only charging the silicon anode partially (<1200 mAh g^{-}

[1]).[18] What is needed in research is to develop a scalable method to synthesize micron-size germanium-based anode materials with reasonable thickness (~100 μm) for practical applications, which can also be charged and discharged to its full capacity with satisfying cycling performance.

Asymmetric reverse osmosis (RO) and nanofiltration (NF) membranes are playing an important role in our daily life by providing billions of tons of desalinized water worldwide annually.[21] These membranes are characteristic of robust asymmetric porous structure consisting of interconnecting nanopores and macropores, [22] which characteristic can be utilized to solve the volume expansion problem of alloying anode materials, e.g., Si and Ge, for next generation high capacity lithium ion battery (LIB). In addition, these membranes can be fabricated in large scale with highly controllable thickness using a well-established roll-to-roll process via a self-assembly phase inversion mechanism.[22, 23] Such an excellent scalability is highly desirable for practical applications in battery industry. In phase inversion process, a homogeneous polymeric solution is immersed into a non-solvent. The polymer has negligible solubility in the non-solvent, while the non-solvent and solvent are miscible with each other. Then de-mixing will occur, resulting in the formation of two phases (polymer-lean and polymer-rich) and the spontaneous generation of asymmetric porous structure (**Figure 1d)**. It is called 'asymmetric membrane' because these membranes consist of a top nano-porous layer and a bottom macro-porous layer (**Figure 1a**). On the top surface, the polymeric solution is in contact with large quantity of non-solvent, leading to a fast de-mixing and quick precipitation of polymer. Thereby the top surface is relatively dense. In stark contrast, the solvent in the bottom layer of polymeric solution is slowly de-mixing with non-solvent, causing the formation of macro-porous structure. [24, 25]

In this report, the scalable membrane technology is adapted to produce polysulfone/Ge composite membranes using Ge micron-size powders as the starting material. These composite membranes are then carbonized to form Ge-C inorganic asymmetric membranes for high performance LIB anodes. These membrane electrodes demonstrate excellent rate and cycling performance owing to the robust interconnecting porous structure and high electrical conductivity. This work is distinguished from other methods in simplicity, efficiency and high scalability.

Results and discussion

Design and fabrication of Ge asymmetric membrane for lithium ion anodes

Due to the large volume change (~260%) and poor mechanical strength, LIB anodes made of micron-size Ge powders have unsatisfying cycling life.[26, 27] Various kinds of nano-structuring (nanowires and nanoparticles) have been proposed to stabilize Ge-based alloying anode. However the manufacturing cost of nanomaterials can be several orders of magnitude higher than micron-size materials because of the use of costly chemical vapor deposition (CVD) technique, expensive catalysts and complex templating methods as mentioned above.[13, 28, 29] Further, graphene, carbon nanotubes and non-conventional binders are usually needed during the preparation of Ge nanoparticles (NPs)-based electrodes.[27, 29, 30] All these facts can significantly hinder their practical applications in large scale. So what is needed is to create a new synthetic route to obtain stable Ge electrodes using micron-size powders as the raw material, thus substantially reducing the cost. Polymeric asymmetric membranes can be fabricated in large scale via a self-assembly phase inversion mechanism.[22, 31] During the phase inversion, a homogeneous polymeric solution of single phase is immersed into a non-solvent, leading to de-mixing and spontaneous formation of asymmetric porous structure. Herein we adapted this amazingly facile method to make inorganic Ge asymmetric membranes for efficient lithium storage (**Figure 1**).

As-received Ge powders (~100 μm) were ground to ~5 μm using a ball mill before being used for the membrane fabrication (**S1**). This grinding process is necessary because 100 μm particles can settle quickly to the bottom of

container due to the effect of gravity, resulting in their separation from the polymeric solution. Ground Ge powders were mixed with carbon black and polysulfone dissolved in N-methyl-2-pyroolidone (NMP), which was then used for the phase inversion. NMP, water and polysulfone (PS) are employed as solvent, non-solvent and polymer, respectively. Carbon black (CB) is utilized as a filler to increase the electrical conductivity and adjust content of active material Ge powders in the membrane to reduce the overall volume expansion. These inorganic/polymeric membranes were carbonized to obtain conductive Ge membranes for LIB anode. Noteworthy, the top dense layer can help prevent the pulverized germanium particles from being leaked out into electrolytes, which can cause rapid and permanent capacity loss. The bottom porous layer can function as a robust mechanical support and allow for the large volume expansion. Further, the layer of carbon film coated on Ge powders can assist the formation of a stable SEI layer and favor a longer cycle life.[32, 33] It is notable this method can be easily scaled up as evident by the 13-inch long Ge asymmetric membrane prepared using a large glass plate as the substrate (**Figure 1**). With roll-to-roll processing facilities in membrane industry, these membranes can be produced continuously in large quantities.

Characterization of germanium asymmetric membranes

As-received Ge powders have a broad size distribution ranging from several microns to hundreds of microns (**S1**). After the grinding process, the size of Ge powders is reduced to 5 μm on average (**S1**). Since these Ge powders have irregular shapes, we use Heywood diameter to represent their size, which was calculated as ($d_p = 2\sqrt{\frac{A}{\pi}}$). Heywood diameter, d_p is the equivalent diameter of the circle that has the same area as the projected area (A) of Ge particle from TEM image (**S1**). The average Heywood diameter is 5.0 μm with a standard deviation of 3.2 μm. In comparison CB NPs are much more uniform with an average diameter of ~56.4 nm and a standard deviation of ~15.7 nm (**S1**). Scanning electron microscope (SEM) imaging confirms the formation of porous structure after the phase inversion process (**Figure 2 and S2**).

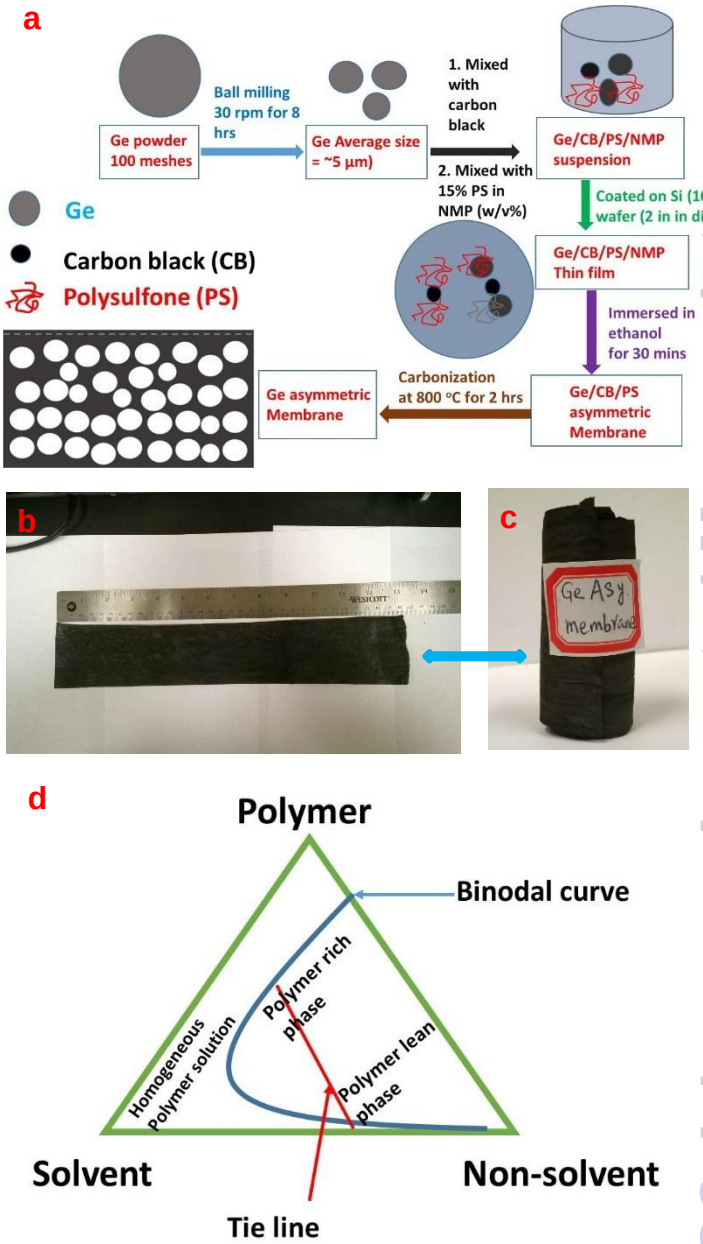

Figure 1. a) Schematic of the fabrication process for germanium asymmetric membranes, b) and c) optical images of a 13-inch long Ge asymmetric membrane and d) the corresponding ternary phase diagram for phase inversion.

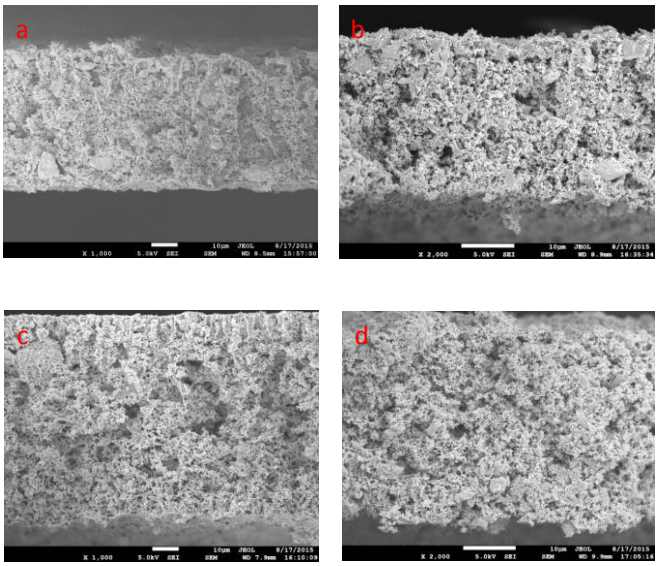

Figure 2. SEM images of (a) Ge asymmetric membrane before carbonization (Ge 15WT100M, 100 µm wet thickness); (b) Ge asymmetric membrane after carbonization at 800 °C for 2 hrs (Ge 15WT100M, 100 µm wet thickness); (c) Ge asymmetric membrane before carbonization (Ge 15WT250M, 250 µm wet thickness); (d) Ge asymmetric membrane after carbonization at 800 °C for 2 hrs (Ge 15WT250M, 250 µm wet thickness). Note: all images are cross-section view.

These Ge micron powders (MPs) are uniformly dispersed in the porous carbon networks (**Figure 2 and S2**). For Ge asymmetric membrane of 100 µm wet coating thickness (Ge 15WT100M), the membrane shrank to 53 µm after the phase inversion because the solvent is de-mixed. After being carbonized at 800 °C for 2 hrs, the membrane thickness was further reduced by 40% to 32 µm (**Figure 2**). For Ge asymmetric membrane of 250 µm wet thickness, the membrane thickness after the phase inversion is 138 µm, which was decreased to 43 µm after the carbonization (**Figure 2**).

The sharp Raman peak centered at 315 cm^{-1} for Ge micron powders and Ge asymmetric membranes carbonized at 800 °C for 2 hrs can be attributed to the phonon scattering of bulk Ge (**Figure 3a**).[34, 35] G and D Raman peaks from graphitic materials can also be seen in these carbonized Ge asymmetric membranes (**Figure 3a**). The low G/D ratio indicates these graphitic materials were not of high crystallinity, which is not surprising due to the low carbonization temperature (800 °C). Powder X-ray diffraction data confirms the presence of crystalline cubic Ge in these carbonized Ge asymmetric membranes (**Figure 3b**). The weak pattern at ~26° is from poorly crystalized graphite, which is also consistent with the low G/D ratio in Raman spectra (**Figure 3a and 3b**).[36] Surface area analysis further verifies the presence of porous structure in these Ge asymmetric membranes (Ge 15WT100M) with a specific area of 132 m^2 g^{-1} calculated using Brunauer–Emmett–Teller (BET) method (**Figure 3c**). These pores have a wide size distribution as proved by Barrett-Joyner-Halenda pore size distribution data (**Figure 3d**). The broad size distribution is also consistent with the SEM imaging and its intrinsic asymmetric structure (**Figure 3d**).

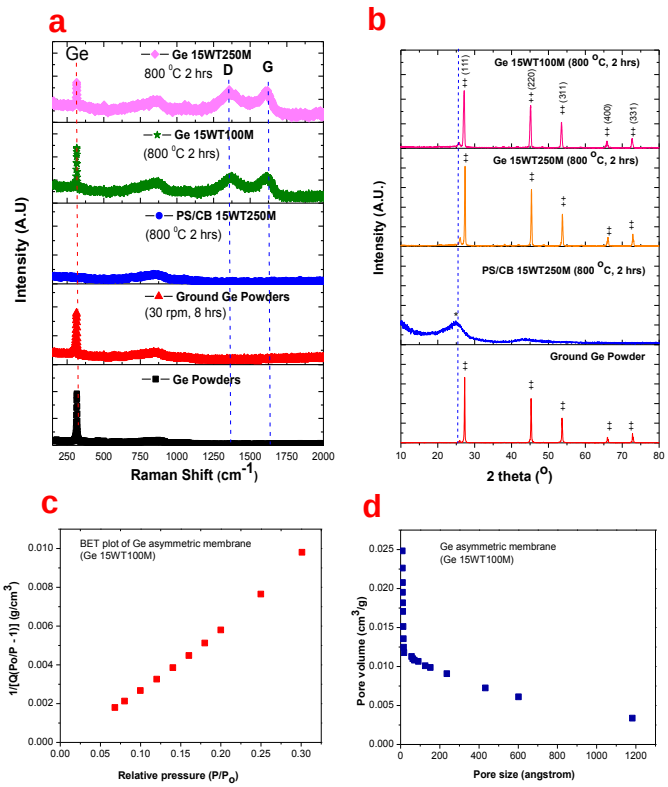

Figure 3. Characterization of Ge asymmetric membranes: (a) Raman Spectra and (b) PXRD patterns of Ge powders, carbonized PS/CB membrane (PS/CB 15WT250M) and Ge asymmetric membranes (Ge 15WT250M and Ge 15WT100M); (c) BET surface area; and (d) BJH pore size distribution of Ge asymmetric membrane (Ge 15WT100M). Note: * is the XRD pattern from graphitic

materials (JCPDS Card No.75- 1621) and ++ represents XRD patterns from cubic phase Ge (JCPDS No. 04-0545). All membranes were carbonized at 800 ºC for 2 hrs.

The content of active material germanium in these carbonized asymmetric membranes was determined using thermogravimetric (TGA) analysis (**Figure 4**) based on an assumption that germanium and carbon can be fully oxidized to GeO_2 (s) and CO_2 (g) in air, respectively. This assumption is validated by TGA data. As shown in **Figure 4**, the mass percentage of pure Ge is increased by 40.1%, indicating the formation of GeO_2. Theoretically, the mass percentage should be increased by 44% if Ge is fully oxidized to GeO_2. The slight difference from theoretical value is probably due to the trivial oxidation of Ge powders during the grinding process. As for carbonized PS/CB membrane, its mass is decreased by 99.8% during the TGA analysis because it is completely oxidized into CO_2 gas. Based on this assumption, the contents of germanium were calculated to be 55.3 and 57.1 wt. % in Ge asymmetric membranes of 100 and 250 μm wet thicknesses (Ge 15WT100M and 15WT250M), respectively.

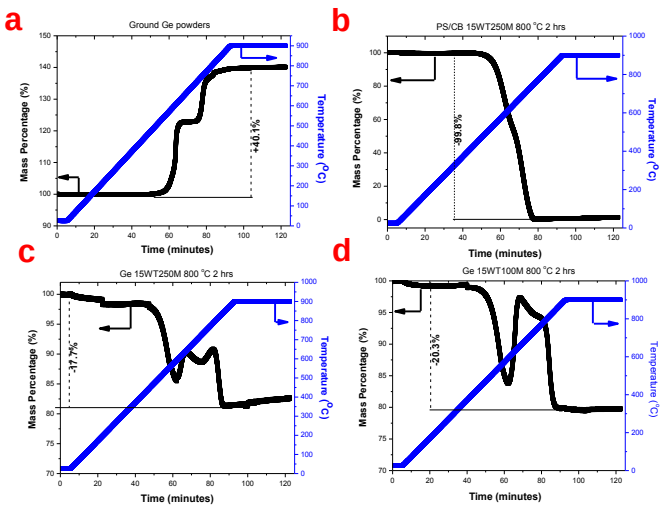

Figure 4. Thermogravimetric analysis of (a) ground Ge powders; (b) carbonized PS/CB 15WT250M membrane; (c) carbonized Ge 15WT250M membrane; and (d) carbonized Ge 15WT100M membrane.

Electrochemical properties of Ge and Ge/carbon black asymmetric membranes as LIB anodes

The de-lithiation capacity of Ge asymmetric membranes carbonized at 800 ºC for 2 hrs with a wet thickness of 100 μm is as high as 1700 mAh g^{-1} at a current density of 200 mA g^{-1} based on germanium (**Figure 5a and 5e**), which is very close to the value reported by Fultz et al..[37] The capacity based on overall membrane mass is ~940 mAh g^{-1}, which is nearly three times higher than commercial graphite electrodes (**Figure 5e**). The electrodes also exhibit excellent rate performance. When applying a current density of 800 mA g^{-1}, nearly 66% (1129 mAh g^{-1} based on Ge mass or 620 mAh g^{-1} based on overall membrane mass) capacity can be retained as compared to 200 mA g^{-1} (**Figure 5e**). Noteworthy, the lithiation and de-lithiation current densities are identical. Such an excellent rate performance can be attributed to the networking carbon structure and high porosity, which allow for excellent electrical conductivity and short lithium ion diffusion length.

Germanium asymmetric membrane electrodes also demonstrate an outstanding cyclability as compared to other micron-size germanium anodes which are not specially treated to obtain nanoscale sub-structures.[10, 20] 70% capacity (850 mAh g^{-1} based on Ge mass or 467 mAh g^{-1} based on overall membrane mass) can be retained after 100 cycles at 600 mA g^{-1} based on Ge mass with a Coulombic efficiency ranging from 99-100 % (**Figure 5a and 5c**). After deducting the capacity from carbon black and carbonized ploysulfone (~200 mAh^{-1} on average), it is still above 750 mAh g^{-1} based on Ge mass (**Figure 5a and 5c**). The capacity is also plotted as normalized to the total electrode weight in Figure 5c and 5e, which provide more information on the overall electrode performance. Although the capacity is much lower when normalized to the total electrode weight, it is still much higher than graphite anode. Noteworthy the capacity could be further increased with optimization of electrode formulation. It is believed the solid asymmetric porous structure can stand the huge stress generated during the germanium lithiation/de-lithiation processes. Furthermore, fractured Ge powders can be retained in these interlinking nanopores and macropores without

being leaked out into the electrolytes and losing capacity rapidly.

During the first formation cycle of 100 μm Ge asymmetric membrane, there are two sharp peaks at 0.21 V and 0.51 V (**S3**), which can be assigned to the insertion and extraction of lithium in crystalline germanium, respectively.[38] In the second and third formation cycles, these two peaks are changed to two broad ones centered at 0.20 V and 0.60 V, respectively, which is due to the insertion and extraction of lithium into amorphorized Ge and is common in germanium anode materials.[39] The initial capacity losses (ICL) of Ge asymmetric membranes are 26% and 30%, respectively, for membranes with wet thicknesses of 100 and 250 μm, respectively. These ICL values are again very comparable to other Ge-based LIB anodes.[16, 40] Thickness of Ge asymmetric membranes has a certain impact on their cycling performance (**Figure 5a**). When the thickness is reduced from 250 to 100 μm (wet membrane thickness), retention rate is improved from 63% to ~70% in 100 cycles. It is probable that the stress in thicker membrane electrode is higher than thinner one, thus tending to destroy the porous structure more easily.

Pure germanium powder electrode is extremely unstable as evidenced by the quick degradation in capacity that was decreased below 100 mAh g^{-1} in less than ten cycles (**Figure 5a and 5b**). Lu, et al. reported the stability of germanium oxide thin film electrode is in reverse proportion to its particle size. For macro-size GeO_2, its initial capacity is only 225 mAh g^{-1}, 30% of which can be retained in 10 cycles.[41] Their data are quite consistent with our pure germanium powder electrode data. When the size increases to microns In contrast carbonized polysulfone and carbon black membrane (PS/CB 15WT250M) without germanium powders shows an excellent cyclability, but unfortunately its capacity is too low (~200 mAh g^{-1}) similar to literature report.[42]

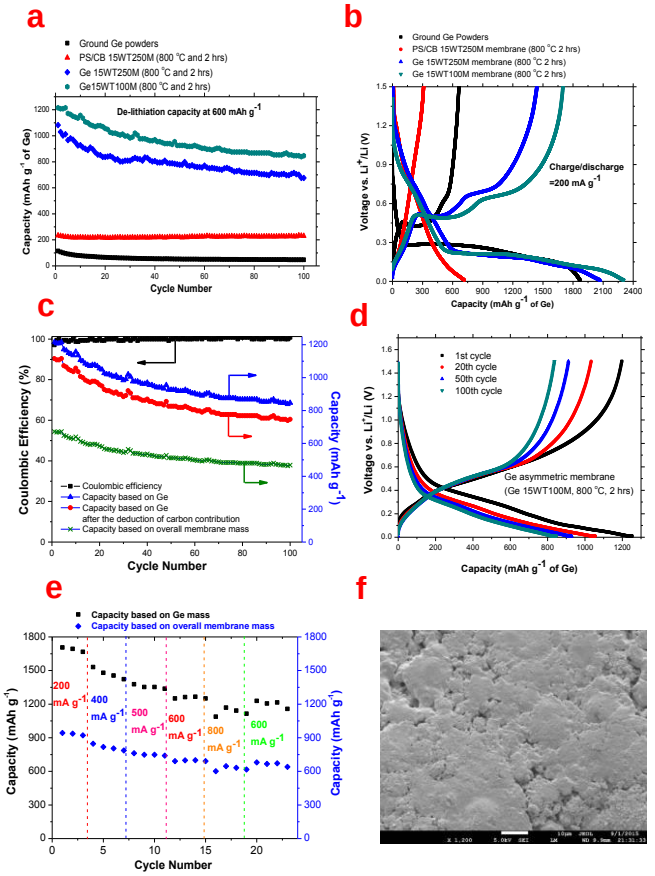

Figure 5. Electrochemical performance of Ge asymmetric membrane electrodes: (a) cycling performance and (b) voltage profiles of Ge asymmetric membranes with wet thicknesses of 100 and 250 μm and carbonized at 800 °C for 2 hrs; (c) Coulombic efficiency and cycling performance of Ge asymmetric membrane of 100 μm thickness; (d) voltage profile of Ge asymmetric membrane electrode of 100 μm thickness at 1st, 50th and 100th cycles; (e) rate tests of Ge asymmetric membrane electrode of 100 μm thickness and f) SEM image of the Ge asymmetric membrane electrode of 100 μm thickness at 100th cycle. Note: ground Ge powders and carbonized CB/PS membrane electrodes are also tested for comparison. The capacities based on overall membrane mass are also provided for better comparison in Figure 5c and 5e.

Experimental

Synthesis of germanium asymmetric membranes using micron-size Ge powders

As-received Ge powders (Alfa Aesar, 100 meshes, 99.999%) were ground for 8 hrs at 30 rpm using a planetary ball mill mixer (Across International, PQ-N04) before being used for the membrane fabrication. Next, 1.0 g ball-milled Ge powders (an average size of ~5 μm), 0.40 g carbon black (TIMCAL SUPER C45 with a

surface area of 45 m^2 g^{-1}) and 1.5 g polysulfone (M_n=22,000, Sigma Aldrich) were dispersed in 10 mL N-methyl-2-pyrrolidone (NMP) (Sigma Aldrich, >99.5%). The solution was mixed thoroughly by vortexing (Barnstead International) for 30 minutes and sonication (Bransonic CPX3800H) for 1 hr. Next, the suspension was coated onto a piece of silicon (100) wafer of 2 inches in diameter using a doctor blade with a wet membrane thickness of either 250 μm or 100 μm. The coated wafer was immersed into ethanol for 30 minutes to form asymmetric membrane. Finally, the membrane was carbonized at 800 °C for 2 hrs using a Lindberg/Blue M™ 1100°C tube furnace with a ramp of ~60 °C min^{-1}. High purity helium gas (99.9999%, Airgas He UHP300) was flown at 200 sccm to prevent oxidation of Ge and carbon. The membranes were labeled as Ge 15WT250M and Ge 15WT100M for wet membrane thicknesses of 250 and 100 μm, respectively. It should be pointed out specifically that asymmetric membrane structure can't be maintained after being carbonized without the addition of carbon black as the filler to support the backbone of the porous structure. The addition of carbon black also benefits the electron transfer and reduces the overall volume change of asymmetric membrane during lithiation/de-lithiation process.

Synthesis of asymmetric membranes without Ge powders

Membranes without Ge powders were also fabricated using the aforementioned method for control experiment, which had a wet membrane thickness of 250 μm and were carbonized at 800 °C for 2hrs. The control membrane sample was labeled as PS/CB 15WT250M herein.

Characterization

A Field Emission Electron Microscopy (JEOL JSM-7600F) attached with Transmission Electron Detector (TED) at Georgia Southern University was utilized for morphology and structural characterization. A Thermo Scientific DXR SmartRaman Spectrometer in Prof. Rafael Quirino labs at Georgia Southern University was used for phase identification. The power of the laser is 3 mW of 532 nm wavelength and the objective lens is ×10 with a total integration time of 100 seconds. Samples were also characterized using powder X-ray diffractometer (Scintag XGEN-4000) using a Cu K_α radiation (λ=1.542 Å) from 10 to 80° with a step rate of 0.03°/s. The acceleration voltage and current are 40 kV and 40 mA, respectively with a step rate of 0.03°/s. A Micromeritics ASAP 2020 Surface Area and Porosimetry Analyzer was employed to measure the specific surface area and pore size distribution. They were calculated using Brunauer-Emmett-Teller (BET) and Barrett-Joyner-Halenda (BJH) methods, respectively. Membrane samples were degassed at 50 μTorr and 300 °C for 30 minutes before N_2 gas adsorption and de-adsorption measurements. The nitrogen adsorption and desorption isotherms were collected at 77 K using ultrahigh purity N_2 gas (Airgas UHP300, 99.9999%). The content of germanium was determined by a thermogravimetric analyzer (NETXSCH STA 449 F3) using compressed air as the purging gas (Ultra Zero, Airgas). The flow rate of compressed air gas is 40 mL min^{-1} and the temperature is ramped at a rate of 10 °C/ min.

Electrochemical evaluation of germanium asymmetric membranes as LIB Anodes

Ge asymmetric membrane was glued directly onto a piece of copper disc (15 mm in diameter and 11 μm thick from MTI Corporation). The glue was made of 0.1 g carbon black and 0.1 g polyvinylidene difluoride (PVDF, MTI Corporation) dissolved in 3 mL NMP. The uncalendered electrode was then dried under vacuum at 120 °C overnight to remove NMP and H_2O moisture. The final mass of active material on the copper disc was ~1.0 mg. The electrode was then assembled into 2032-type coin cells using lithium metal (EQ-Lib-LiC25, MTI Corporation) as the counter electrode and 1 M $LiPF_6$ dissolved in ethylene carbonate (EC), dimethyl carbonate (DMC) and diethyl carbonate (DEC) with a volume ratio of 1:1:1 (MTI Corporation) as the electrolyte. Inside the glove box (LCPW, LC Technology Solutions, INC.), oxygen and water

concentrations were maintained below 1 ppm. The membrane separator was purchased from MTI Corporation (ethylene/polypropylene blend with pore sizes 20-30 nm). Two control samples, ball-milled Ge powders (an average size of ~5 μm) and asymmetric membrane without Ge powders (PS/CB 15WT250M) were also assembled into coin cell batteries for comparison. Asymmetric membrane without Ge powders was assembled into coin cell battery using the same method as the one for Ge asymmetric membrane. In the case of ball-milled Ge powders, they were first mixed with carbon black and PVDF in a mass ratio of 8:1:1 to make a uniform slurry, and then coated onto a copper disc with a wet thickness of 100 μm. Other steps are same as those for Ge asymmetric membrane electrode. Galvanostatic cycling tests of LIB half-cells were conducted using a multi-channel Potentiostat/EIS (BIO-LOGIC VMP3) at 20 ºC. The voltage window is 0.01~1.50 V (vs. Li^+/Li). Three formation cycles at 200 mA g^{-1} were performed on all LIB cells before any rate and cycling performance tests. Same current densities were applied for both charging and discharging processes for the rate tests.

Conclusions

It is demonstrated that asymmetric porous structure can be utilized as a backbone for lithium-ion battery electrode, where the interconnecting nanopores and macropores mitigates the volume expansion problem of alloy anode materials. This method provides a facile technique toward roll-to-roll manufacturing of high capacity alloy anodes. In addition, it shows that commercially available micron-size Ge powders can be used as the starting material for high capacity LIBs and deliver highly stable cycling performance, which is attributed to the asymmetric porous structure providing both mechanical support and free volume to accommodate Ge lithiation and de-lithiation with large volume variation. It is also believed that the unique interlinking nanopores and macropores can efficiently prevent the loss of pulverized Ge powders and also enhance the lithium diffusion rate by providing multiple diffusion channels. While the manufacturing process poses commercial potential, challenges remain and further developments in lowing material cost, increasing cycling performance and areal material loading are required.

Acknowledgements

JW deeply appreciates the financial and infrastructural supports from Georgia Southern University, especially the sustainability fee grant. We thank Dr. Cliff Padgett for his help and use of the PXRD at Armstrong State University and Dr. Quirino for the use of Raman spectroscopy.

Notes and references

[a] Department of Chemistry, Georgia Southern University, 250 Forest Drive, Statesboro, GA, 30460, USA
[b] Department of Biology, 75 Georgia Avenue, Statesboro, GA, 30460, USA
[c] Energy & Transportation Science Division, Oak Ridge National Laboratory, Oak Ridge, TN, 37831, USA

† Footnotes should appear here. These might include comments relevant to but not central to the matter under discussion, limited experimental and spectral data, and crystallographic data.

Electronic Supplementary Information (ESI) available: [details of any supplementary information available should be included here]. See DOI: 10.1039/b000000x/

References:

1. J. M. Tarascon and M. Armand, *Nature*, 2001, **414**, 359-367.
2. B. Scrosati, *Electrochimica Acta*, 2000, **45**, 2461-2466.
3. J. B. Goodenough and Y. Kim, *Chemistry of Materials*, 2010, **22**, 587-603.
4. G. Cui, L. Gu, L. Zhi, N. Kaskhedikar, P. A. van Aken, K. Müllen and J. Maier, *Advanced Materials*, 2008, **20**, 3079-3083.
5. D. A. Stevens and J. R. Dahn, *Journal of The Electrochemical Society*, 2000, **147**, 1271-1273.
6. K. McCormac, I. Byrd, R. Brannen, B. Seymour, J. Li and J. Wu, *physica status solidi (a)*, 2015, **212**, 877-881.
7. L. Baggetto and P. H. L. Notten, *Journal of The Electrochemical Society*, 2009, **156**, A169-A175.
8. L. Y. Lim, N. Liu, Y. Cui and M. F. Toney, *Chemistry of Materials*, 2014, **26**, 3739-3746.
9. K. H. Seng, M. H. Park, Z. P. Guo, H. K. Liu and J. Cho, *Angewandte Chemie International Edition*, 2012, **51**, 5657-5661.
10. W. Liang, H. Yang, F. Fan, Y. Liu, X. H. Liu, J. Y. Huang, T. Zhu and S. Zhang, *ACS Nano*, 2013, **7**, 3427-3433.
11. M. Gu, Y. Li, X. Li, S. Hu, X. Zhang, W. Xu, S. Thevuthasan, D. R. Baer, J.-G. Zhang, J. Liu and C. Wang, *ACS Nano*, 2012, **6**, 8439-8447.
12. J. N. Weker, N. Liu, S. Misra, J. C. Andrews, Y. Cui and M. F. Toney, *Energy & Environmental Science*, 2014, **7**, 2771-2777.
13. C. K. Chan, X. F. Zhang and Y. Cui, *Nano Letters*, 2008, **8**, 307-309.

14. M.-H. Park, Y. Cho, K. Kim, J. Kim, M. Liu and J. Cho, *Angewandte Chemie*, 2011, **123**, 9821-9824.
15. R. Mukherjee, R. Krishnan, T.-M. Lu and N. Koratkar, *Nano Energy*, 2012, **1**, 518-533.
16. J. Liang, X. Li, Z. Hou, T. Zhang, Y. Zhu, X. Yan and Y. Qian, *Chemistry of Materials*, 2015, **27,** 4156–4164
17. K. C. Klavetter, S. M. Wood, Y.-M. Lin, J. L. Snider, N. C. Davy, A. M. Chockla, D. K. Romanovicz, B. A. Korgel, J.-W. Lee, A. Heller and C. B. Mullins, *Journal of Power Sources*, 2013, **238**, 123-136.
18. L.-F. Cui, L. Hu, H. Wu, J. W. Choi and Y. Cui, *Journal of The Electrochemical Society*, 2011, **158**, A592-A596.
19. H. Wu, G. Yu, L. Pan, N. Liu, M. T. McDowell, Z. Bao and Y. Cui, *Nat Commun*, 2013, **4,** 1943.
20. C. Wang, H. Wu, Z. Chen, M. T. McDowell, Y. Cui and Z. Bao, *Nat Chem*, 2013, **5**, 1042-1048.
21. L. F. Greenlee, D. F. Lawler, B. D. Freeman, B. Marrot and P. Moulin, *Water Research*, 2009, **43**, 2317-2348.
22. M. T. Domínech-Carbó and E. Aura-Castro, *Stud Conserv*, 1999, **44**, 19-28.
23. P. Radovanovic, S. W. Thiel and S.-T. Hwang, *Journal of Membrane Science*, 1992, **65**, 231-246.
24. H. Strathmann, K. Kock, P. Amar and R. W. Baker, *Desalination*, 1975, **16**, 179-203.
25. D. M. Koenhen, M. H. V. Mulder and C. A. Smolders, *Journal of Applied Polymer Science*, 1977, **21**, 199-215.
26. J. Nelson Weker, J. C. Andrews, Y. Cui, W. Chueh and M. F. Toney, *Microscopy and Microanalysis*, 2014, **20**, 1526-1527.
27. K. Mishra, W. Xu, J. Xiao, R. Cao, M. H. Engelhard, J. Zhang and X.-D. Zhou, *Meeting Abstracts*, 2015, **MA2015-03**, 549.
28. T. Kennedy, E. Mullane, H. Geaney, M. Osiak, C. O'Dwyer and K. M. Ryan, *Nano Letters*, 2014, **14**, 716-723.
29. H. Tian, F. Xin, X. Wang, W. He and W. Han, *Journal of Materiomics*, DOI: http://dx.doi.org/10.1016/j.jmat.2015.06.002.
30. J. Cheng and J. Du, *CrystEngComm*, 2012, **14**, 397-400.
31. G. R. Guillen, Y. Pan, M. Li and E. M. V. Hoek, *Ind. Eng. Chem. Res.*, 2011, **50**, 3798–3817.
32. H. Wu, G. Chan, J. W. Choi, I. Ryu, Y. Yao, M. T. McDowell, S. W. Lee, A. Jackson, Y. Yang, L. Hu and Y. Cui, *Nat Nano*, 2012, **7**, 310-315.
33. N. Liu, H. Wu, M. T. McDowell, Y. Yao, C. Wang and Y. Cui, *Nano Letters*, 2012, **12**, 3315-3321.
34. M. M. Rzaev, T. M. Burbaev, V. A. Kurbatov, N. N. Melnik, M. Mühlberger, A. O. Pogosov, F. Schäffler, N. N. Sibeldin, V. A. Tsvetkov, P. Werner, N. D. Zakharov and T. N. Zavaritskaya, *physica status solidi (c)*, 2003, **0**, 1262-1266.
35. J. V. Smagina, V. A. Zinoviev, P. L. Novikov, V. A. Armbrister, E. S. Koptev and A. V. Dvurechenskii, *Journal of Physics: Conference Series*, 2010, **245**, 012071.
36. A. Magasinski, P. Dixon, B. Hertzberg, A. Kvit, J. Ayala and G. Yushin, *Nat Mater*, 2010, **9**, 353-358.
37. J. Graetz, C. C. Ahn, R. Yazami and B. Fultz, *Journal of The Electrochemical Society*, 2004, **151**, A698-A702.
38. A. M. Chockla, K. C. Klavetter, C. B. Mullins and B. A. Korgel, *ACS Applied Materials & Interfaces*, 2012, **4**, 4658-4664.
39. N. Nitta and G. Yushin, *Particle & Particle Systems Characterization*, 2014, **31**, 317-336.
40. X. Gao, W. Luo, C. Zhong, D. Wexler, S.-L. Chou, H.-K. Liu, Z. Shi, G. Chen, K. Ozawa and J.-Z. Wang, *Scientific Reports*, 2014, **4**, 6095.
41. J. K. Feng, M. O. Lai and L. Lu, *Electrochimica Acta*, 2012, **62**, 103-108.
42. L. Fransson, T. Eriksson, K. Edström, T. Gustafsson and J. O. Thomas, *Journal of Power Sources*, 2001, **101**, 1-9.